Analysis of Highly Directive Cavity-Type Configurations Comprising of Low Profile Antennas Covered by Superstrates

Nader FARAHAT [1], *Raj MITTRA* [2], *Katherine LUGO* [1], *Lai-Ching MA* [2], *Rodney A. GOMEZ* [1]

[1] Dept. of Electrical Engineering, Polytechnic University of Puerto Rico, P.O. box 192017 San Juan, PR 00919
[2] Electromagnetic Communication Laboratory, 319 EE East The Pennsylvania State University, University Park, PA 16802

nader.farahat@gmail.com, mittra@engr.psu.edu, katherinelugo@ieee.org, lum116@psu.edu, rodneyg@ieee.org

Abstract. *In this paper we present a technique for designing antenna/superstrate composites to produce enhanced directivities. As a first step, we study the underlying mechanism that governs the performance of theses antennas by studying the canonical problem of a line source in a rectangular waveguide. The above problem is solved by constructing the Green's function corresponding to the line source in the rectangular guide, one of whose walls is partially reflecting, that is can leak electromagnetic energy into the space external to the guide. The Green's function for this problem can be constructed by aggregating the multiple reflections from the two walls. Although the above model is only two-dimensional, we show that it can be used to predict the performance of antenna/superstrate composites. We demonstrate this by modeling several highly directive antennas and show that indeed the required characteristics of this type of antennas can be determined from the analysis of the cutoff behavior of the rectangular guide.*

Keywords

Highly directivity antennas, frequency selective surfaces.

1. Introduction

In recent years the design of highly directive cavity-type antennas has drawn considerable attention of researchers in the field of antenna technology [1-3]. These composites comprise of low gain antennas, such as microstrip patches or printed dipoles, covered by Electromagnetic Band Gap (EBG) structures or Frequency Selective Surfaces (FSS), to achieve a high directivity. In contrast to parabolic reflectors, for instance, these composites are low profile as well as compatible with the integrated circuits. The underlying mechanism of the directivity enhancement of such composites has been interpreted from different perspectives, such as defect modes in photonic crystals, low index metamaterials, leaky wave antennas and cavity resonator modes, [1-3]; however, a clear and unified explanation of the performance of composite is yet to be found. We investigate several examples of such antennas in this paper that not only provide us a clear understanding but also help us develop improved designs. Furthermore, it is helpful to gain an understanding of the fundamental limits of these antennas, and this is facilitated by the analysis presented herein. For instance, without a theoretical understanding of the gain-enhancing phenomenon, many practical design issues such as controlling the losses (ohmic and dielectric), impedance matching and achieving the frequency bandwidth cannot be addressed. Once the analysis alluded to above has been carried out, the design and optimization process of efficient and practical antennas can follow.

We first analyze a two-dimensional model of two parallel plates, excited by a line source located inside the plates, as illustrated in Fig. 1. Though simple, this model provides us an insight into the physical phenomenon that describes the field behavior inside the cavity formed by the ground plane of the microstrip patch antenna and the superstrate. It should be noted that the only way power can leak out of the cavity is through the Partially Reflective Surface (PRS). Furthermore, the far-field pattern of an aperture is related to the Fourier transform of its field distribution; consequently, the spectral solution of the Green's function, sampled on the surface, above the superstrate can be used to predict the far-field pattern of the antenna. Although, we will ignore the issue of input impedance of the source for the time being, we will show later that the power reflected from the superstrate into the feed line of the dipole or microstrip patch can produce a high standing wave ratio and large impedance mismatch.

Following the study of the 2-D model we turn now to the investigation of practical antennas and study the field distributions and far-field patterns at frequencies in the vicinity of the resonant frequency of the composite. The objective of this study is to develop a systematic technique for designing an efficient - as well as practical - highly directive antenna-FSS composite, based on the understanding of the directivity enhancement phenomenon we have gained from the simpler 2-D model. Toward this end, we begin by studying the existing designs that have already been found successful, they were based on either numerical modeling or measurements. After carrying out the simulations, we extract the parameters of interest such as gain, return loss, far-field pattern, etc. Furthermore, we study the field distribution inside the cavity, which is formed by antenna ground plane and the superstrate, to understand the behavior of this type of antennas. Our studies have led us to conclude that the simple 2-D model provides us valuable clues for the understanding the general performance of the 3-D configurations. To model the 3-D antenna composites, we use the Finite Difference Time Domain (FDTD) method [4], which has been used extensively for the simulation of antenna configurations [5]. The FDTD obtains the response across the frequency of interest band in a single simulation rather than running the simulation one frequency at a time, as is the case of the frequency domain methods. A modification to the basic FDTD algorithm also enables us to analyze the frequency-independent (dispersive) material that we might employ for the superstrate. In particular, the FDTD method provides an efficient way of handling infinite periodic structures when the periodic boundary condition [6] is implemented in it.

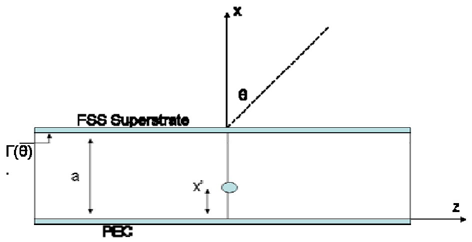

Fig. 1. Illustration of an infinite line source exciting the 2-D cavity-type antenna covered by FSS superstrate with reflection coefficient of $\Gamma(\theta)$=-0.95.

2. Green's Function of Line Source in a Rectangular Waveguide

We start with a 2-D model of excitation of a rectangular waveguide by an infinite line source. This model (see Fig. 1) can also be viewed as a 2-D cavity-type antenna with PRS, if the upper wall is not a perfect electric conductor (PEC) and, hence, can leak out electromagnetic fields into the space above. Let an infinite line source along the y-direction, located at $x=x'$, excite the 2-D cavity-type antenna covered by an FSS superstrate with a reflection coefficient of $\Gamma(\theta)$. The Fourier transform of the Green's function for this geometry, with respect to the z-coordinate, i.e., $f(x, kz)$ is calculated by adding the contributions of the multiple reflections of the primary fields, as an infinite series, following the procedure given in [7], assuming that both the plates above and below are PEC. It has also been shown in [7] that the series can be summed up in a closed form [7]. Next, we modify the series by assuming that the upper plate has the reflection coefficient slightly less than -1, Γ=-.095 in our example, and reevaluate the series numerically. After the convergence has been achieved, which requires the inclusion of approximately 600 terms, we argue that the spectral representation of the Green's function at the top surface of the upper plate $f(x=a,kz)$, is related to the far-field pattern of the antenna.

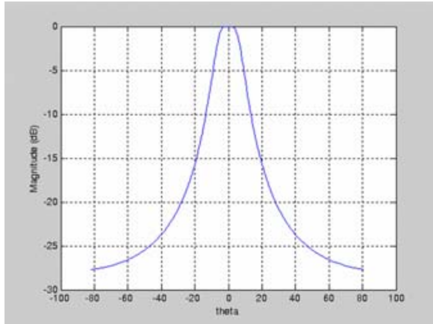

Fig. 2. Normalized far-field pattern at the resonant frequency for the superstrate with Γ=-0.95.

Fig. 2 shows the normalized far-field pattern at the resonant frequency of the cavity $f_0=c/2a$, where c is the speed of light in free space and a is the separation between the plates with Γ=-0.95. For this aperture size, we estimate a directivity of 23 dBi by using the Krauss formula for a square aperture with equal distribution in both planes. The far-field pattern exhibits the corresponding aperture distribution with a tapered amplitude and uniform phase.

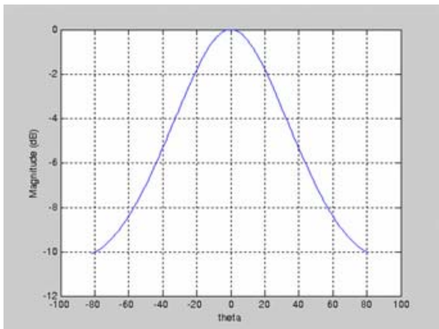

Fig. 3. Normalized far-field pattern at 0.8 of the resonant frequency for the superstrate with Γ= -0.95.

If we decrease the frequency of the operation, the far-field pattern becomes wider, as shown in Fig. 3 for $0.8f_0$, and the estimated directivity falls to 11.5 dBi. The far-field pattern exhibits the aperture distribution with an increased taper in the amplitude though the phase is still uniform, as we surmise from the fact that the maximum of the pattern points toward the zenith. On the other hand, the main lobe of the pattern splits and the directivity deteriorates along the zenith (θ=0) if we go above the resonant frequency f_0, as is evident from Figs. 4 and 5. The patterns now correspond to an aperture distribution with a progressive phase taper, since the beam scans with an increase in the frequency. Further increase of the frequency leads to an excitation of the higher-order harmonics, *TE3* mode for instance, and the pattern now becomes a combination of the scanned lobes of the lower harmonics (*TE1* mode) that are still in the visible range. This may be seen from Fig. 6 for a frequency of $3f_0$, with the *TE3* mode still contributing to the main lobe while the *TE1* lobes are pushed back toward off-center angles. This trend exists for all the higher harmonics and therefore only the first harmonic contributes to the single-lobe that has a high directivity.

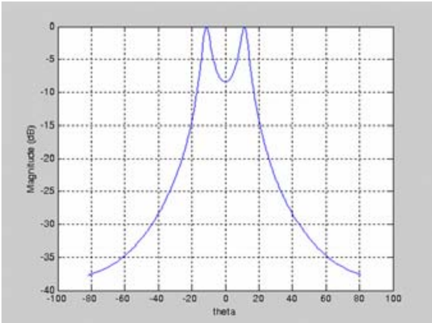

Fig. 4. Normalized far-field pattern at 1.01 of the resonant frequency for the superstrate with Γ= -0.95.

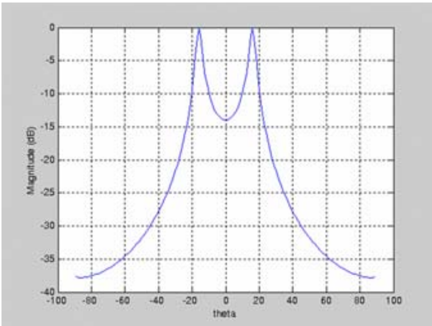

Fig. 5. Normalized far-field pattern at 1.04 times the resonant frequency for the superstrate with Γ=-0.95

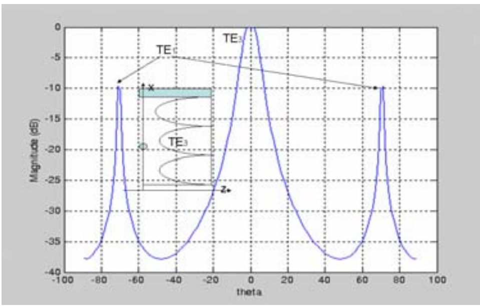

Fig. 6. Normalized far-field pattern at 3 times the resonant frequency for the superstrate with Γ=-0.95.

To study the bandwidth of this cavity, we plot in Fig. 7 the far-fields at zenith (θ=0) for different frequencies. The 3dB bandwidth of 8% is evident from the -3dB border values of 0.96 and 1.04 of the resonant frequency f_0.

To study the effect of the variation of the reflection coefficient of the superstrate with the angle of incidence, we consider a simple dielectric layer (ε_r=7.8, thickness d=0.75cm) as the superstrate. Fig.8 plots the reflection coefficient $\Gamma(\theta)$ vs. frequency at normal incidence as well as the variation as a function of the incident angle at 4.7 GHz. The variation of the far-field pattern vs. the incident angle is essentially the same as that of the constant reflection coefficient case. We have carried out extensive simulations of similar configurations, and have found that the reflection coefficient at normal incidence plays a key role in generating patterns with high directivities.

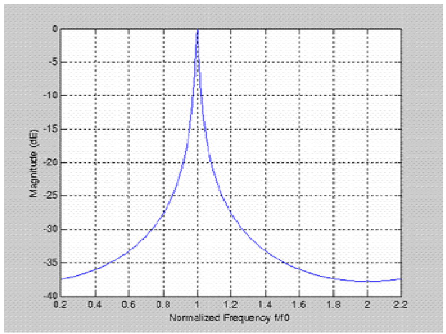

Fig. 7. Normalized fields along the zenith for different frequencies. The 3dB bandwidth is 8 %. f_{min}=0.96 and f_{max}=1.04.

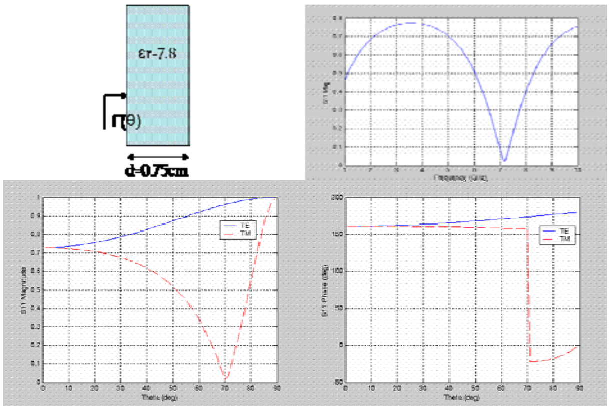

Fig. 8. Illustration of the simple dielectric layer superstrate. Top left: geometry. Top right: reflection coefficient for normal incident. Bottom left: magnitude of the reflection coefficient at 4.7 GHz. Bottom right: phase of the reflection coefficient at 4.7 GHz

3. Parallel Plate Waveguide Interpretation

The results predicted in the previous section can also be obtained by using an alternative approach, which is based on a study of the wave propagation inside the parallel plate waveguide, shown in **Fig. 9.**

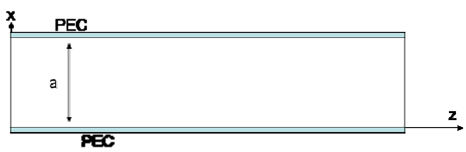

Fig. 9. Illustration of the parallel plate wave guide with TE modes (*Ey, Hx* and *Hz*).

The *TE1* excitation inside this waveguide with *Ey, Hx* and *Hz* components is similar to the one in the cavity problem depicted in Fig. 1. The behaviors of the electric and magnetic fields along the guide are quite similar for both the *TE1* and *TM1* modes [7]. Their field distributions have tapered magnitude and constant phase behaviors below the cutoff frequency $f_0=c/2a$, while these distributions become uniform in magnitude and progressive in phase above the cutoff frequency. The tapered magnitude along the z-direction at a frequency slightly below cutoff, namely $0.96f_0$, as well as the behavior of its Fourier transform vs. angle θ, are shown in Fig. 10. If this field distribution leaks out of the guide, as for instance it would if one of the walls is PRS, it would generate a pattern similar to that of the cavity aperture at the resonant frequency, which is shown in Fig. 2. On the other hand, if we go to a frequency slightly above the cutoff, say $1.04f_0$, we find that the magnitude of the field along the *z*-direction remains constant but its phase exhibits a progressive change. The phase of the field along the *z*-direction at $1.04f_0$ as well as the Fourier transform of the field at the same frequency are plotted in Fig. 11.

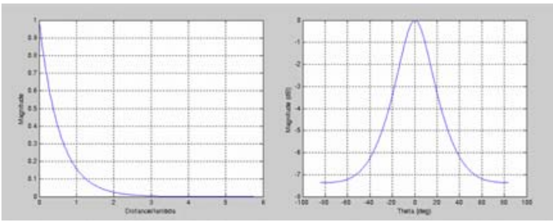

Fig. 10. First mode (TE1 or TM1) magnitude distribution at 0.96 of the cutoff frequency inside the waveguide (left) and its Fourier transform (right).

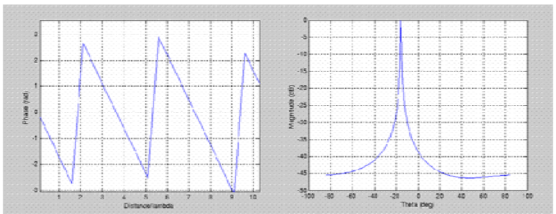

Fig. 11. First mode (TE1 or TM1) phase distribution at 1.04 of the cutoff frequency inside the waveguide (left) and its Fourier transform (right).

Once again, when the waveguide walls have a leakage, the Fourier transform of the field distribution indicates that the far-field pattern points to the same direction, namely 18 degrees, as that for the pattern shown in Fig. 5. Note that there is only one lobe in the pattern plotted in Fig. 11 (right), because we have considered only a single traveling wave inside the guide. It appears that a high directivity is achieved in this structure when it operates at a frequency which is in the close vicinity of the cutoff frequency (resonant frequency in the cavity interpretation), and drops off immediately after that, while the main lobe splits. The magnitude distributions at frequencies below the cutoff have sharper tapers, hence their patterns are wider. The results also show that relatively narrow band widths are associated with this type of antennas that achieve high directivities. On the other hand, in order to allow the leakage a reflection coefficient of the superstrate, should be close to –1.

In the following sections we study the practical designs of highly-directive cavity-type antennas and show that indeed they must operate near-the-cutoff regime, and must have superstrates with high reflection coefficients.

4. Numerical Modeling of Practical Cavity-Type Antennas

We start with the example of a woodpile EBG antenna [2], whose geometry is shown in Fig. 12, and which we simulate via the FDTD method. The rectangular waveguide radiates into a superstrate comprising of 19 woodpile unit cells made from a dielectric medium, with ε_r=9.6. The separation between the woodpiles and the conducting plate (30x30 mm), which serves as a flange for the feeding guide, is 1.5 mm. The *E*-plane far-field patterns for several frequencies are shown in Fig. 13. It is evident that the high directivity (26 dBi) is obtained at the resonant frequency of 95 GHz, and that the main lobe splits at 100 GHz. It is also noted from Fig. 14 that the reflection coefficient, as seen by the waveguide, increases as the operating frequency moves closer to the resonant frequency of 95 GHz, and this, in turn, causes a large standing wave pattern inside the guide, consequently, the return loss of this antenna is high and its gain can be quite low despite its high directivity, unless we utilize a matching circuit to mitigate this problem. We also simulate the woodpile EBG alone when it is illuminated by a normally incident uniform plane wave, and plot its reflection and transmission characteristics in Fig. 15. The figure clearly shows that its reflectivity is high around 95 GHz.

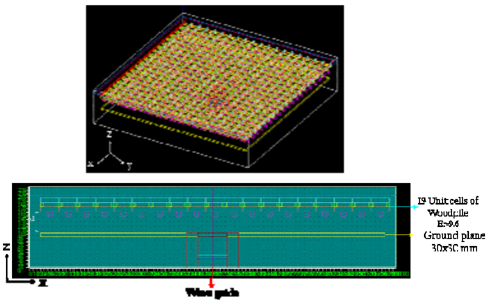

Fig. 12. FDTD simulation of the woodpile EBG (19 unit cells ε_r=9.6) and rectangular waveguide mounted in the conducting plate 30x30 mm and *d*=1.5 mm.

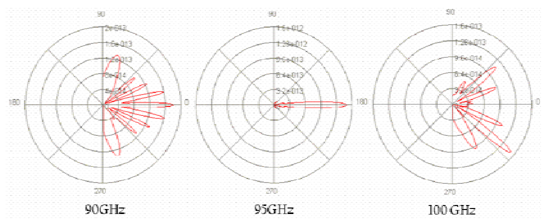

Fig. 13. E-plane far-field pattern of the woodpile EBG antenna at several frequencies. Directivity of 26 dBi is obtained at 95 GHz.

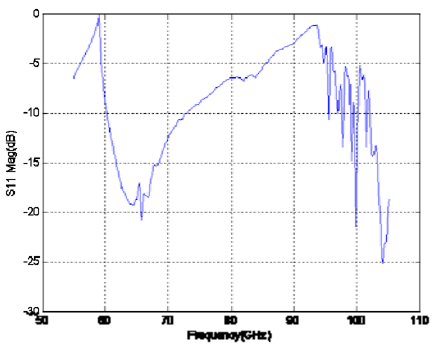

Fig. 14. Reflection coefficient measured inside the rectangular waveguide vs. frequency.

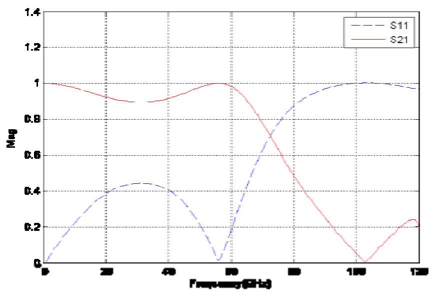

Fig. 15. Reflection and transmission coefficients of the woodpile EBG surface vs. frequency obtained by the periodic FDTD.

For the second example we study the Photonic Band Gap (PBG) antenna described in [1], whose transmission coefficient is shown in Fig. 16 along with the dimensions of the PBG in the inset of the figure.

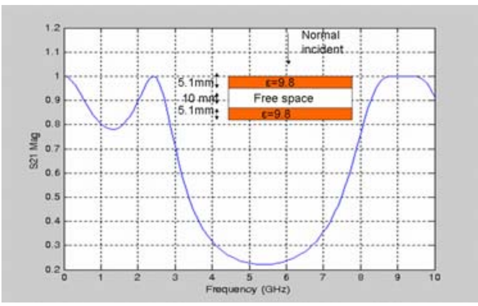

Fig. 16. Transmission coefficient of the PBG surface vs. frequency.

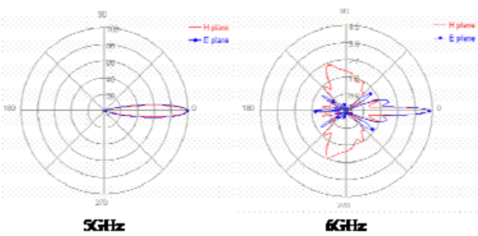

Fig. 17. E- and H- plane far-field patterns of the PBG antenna at 2 frequencies. Directivity of 20 dBi is obtained at 5 GHz.

The operating frequency is 5 GHz, at which the transmission is quite low. A dipole antenna above the conducting plate is covered by this PBG surface [1] and the separation is adjusted for resonance at 5 GHz. The far-field patterns for the frequencies of 5 and 6 GHz are shown in Fig. 17. We note that a maximum directivity of 20 dBi is obtained at 5 GHz, and the behaviors of the pattern follow the same trend described earlier. Figs. 18 to 21 display the co-polar electric field distributions on the surface just above the PBG antenna for several frequencies that span the cutoff and propagating mode regimes inside the antenna. The behaviors of the amplitude and phase distributions are consistent with the interpretations that we have provided previously in the last section.

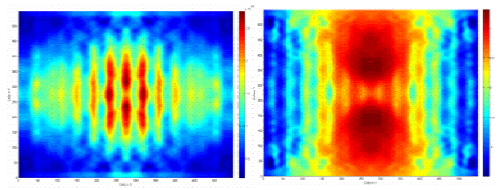

Fig. 18. Co-polar component of electric field on top of the PBG antenna at 1 GHz amplitude (left) and phase (right).

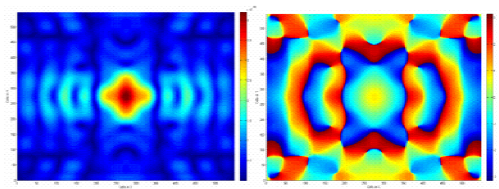

Fig. 19. Co-polar component of electric field on top of the PBG antenna at 4 GHz amplitude (left) and phase (right).

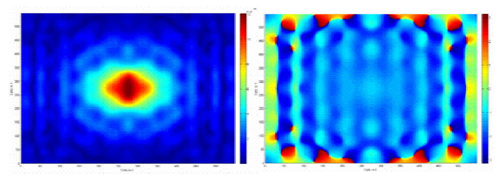

Fig. 20. Co-polar component of electric field on top of the PBG antenna at 5 GHz amplitude (left) and phase (right).

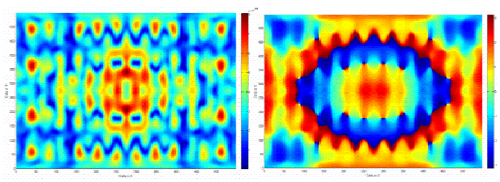

Fig. 21. Co-polar component of electric field on top of the PBG antenna at 6 GHz amplitude (left) and phase (right).

Next, to increase the directivity while keeping the size of the PBG antenna, we use four dipoles that are symmetrically placed in the centers of four squares in the region between the PBG and the conducting ground. The far-field pattern of this four-element array, shown in Fig. 22, achieves a directivity of 22 dBi, which is 2 dB above that of the single- dipole-feed case. It is interesting to note that although the spacing between the dipoles is on the order of 2 wavelengths, the array/superstrate composite has no grating lobes. The field distribution on top of the PBG superstrate is shown in Fig. 23. We observe that the superstrate acts to smooth the amplitude distribution as compared to the corresponding one above a four-element array in the absence of the superstrate, which has peaks and valleys, and whose radiation pattern clearly has grating lobes.

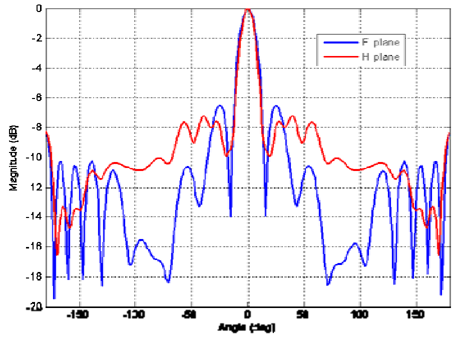

Fig. 22. E- and H- plane far-field patterns of the array of the 4 dipoles inside the PBG antenna at 5 GHz. Directivity of 22 dBi is obtained at 5 GHz.

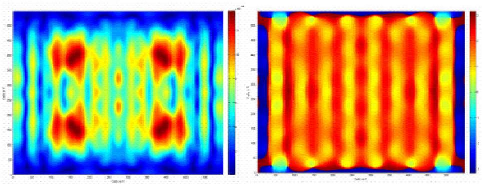

Fig. 23. Co-polar component of electric field on top of the PBG antenna with 4 dipoles at 5 GHz amplitude (left) and phase (right)

For the last example, we turn to the composite antenna with a dipole-FSS [3] type of superstrate. First, we simulate the FSS alone by illuminating it with a normally incident uniform plane wave via the Method of Moments (MoM), as well as with a periodic FDTD code. The reflection coefficient of the FSS, thus obtained, is shown in Fig. 24 and we note that this surface has a high reflectivity at 11 GHz.

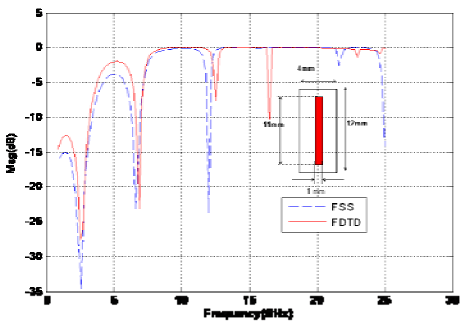

Fig. 24. Reflection coefficient of the dipole FSS surface vs. frequency obtained by the periodic FDTD and MoM

Next we simulate a short radiating dipole placed above a ground plane and covered by the FSS [3], by choosing a separation distance between the ground and the superstrate so as to achieve a resonance at 11 GHz. Finally, we compute the far-field patterns of the composite by using the FDTD method, and plot them as various frequencies in Fig. 25. The maximum directivity of 16 dBi is realized at 11 GHz, and once again we note that the patterns show the trend that we described earlier. In addition, we note that the field distributions above the FSS, shown in Figs. 26-28, are consistent with those predicted by studying the transition behavior as we go from the cutoff to propagating modes.

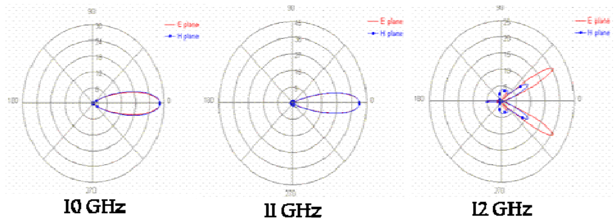

Fig. 25. E-plane far-field pattern of the dipole FSS antenna at several frequencies. Directivity of 16 dBi is obtained at 11 GHz.

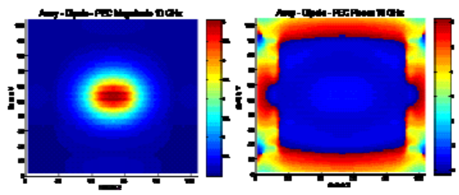

Fig. 26. Co-polar component of electric field on top of the dipole FSS antenna at 10 GHz amplitude (left) and phase (right)

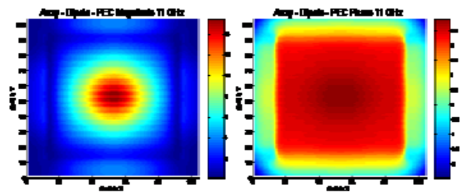

Fig. 27. Co-polar component of electric field on top of the dipole FSS antenna at 11 GHz amplitude (left) and phase (right).

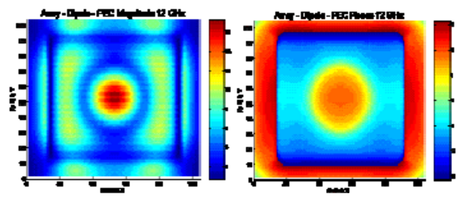

Fig. 28. Co-polar component of electric field on top of the dipole FSS antenna at 12 GHz amplitude (left) and phase (right).

5. Conclusion

The 2-D cavity and parallel plate waveguide models have been used in this work to develop an understanding of the mechanism that leads to the design of highly directive cavity-type antennas. The analysis shows that the highly reflective behavior of the superstrate at normal incidence plays a major role in determining the performance of the antenna composite. The maximum directivity is obtained close to the resonant/cutoff frequency which realizes a uniform phase and smooth amplitude taper in the surface distribution above the superstrate. The split in the main lobe above the resonant frequency is explained in terms of the excitation of the first propagating mode. The results obtained from the simulation of three highly directive antennas show that their behaviors are uniformly consistent with the above interpretations. The patterns of these antennas all become more directive as the frequency approaches the cutoff, though the return loss of the feed line may deteriorate at these frequencies owing to the high reflection into the line from the superstrate. In all of these cases, the propagation mode is launched and the pattern splits into two lobes that scan away from the center as we increase the frequency. The field distributions above the superstrates of these antennas exhibit the same behaviors as those predicted from the simple models of a 2-D cavity and a parallel plate waveguide.

Acknowledgements

This material is based upon work supported by, or in part by, the U. S. Army Research Laboratory and the U. S. Army Research Office under contract/grant number W911NF-06-1-0027.

References

[1] THEVENOT, M., CHEYPE, C., REINEIX, A., JECKO, B. Directive photonic-bandgap antennas. *IEEE Transactions on Microwave Theory and Techniques,* 1999, vol. 47, no. 11.

[2] LUGO, K., GOMEZ, R. A., LEE, Y., FARAHAT, N., MITTRA, R., HAO, Y. *FDTD Analysis of an Antenna Covered by a Dielectric Woodpile EBG Superstrate*. Accepted to AP-S08. San Diego (California), July 2008.

[3] LEE, Y. J., YEO, J., MITTRA, R., PARK, W. S. Design of a high-directivity electromagnetic band gap (EBG) resonator antenna using a frequency selective surface (FSS) superstrate. *Microwave and Optical Technology Letters,* 2004, vol. 43, no. 6, p. 462–467.

[4] YEE, K. S. Numerical solution of initial boundary value problems involving Maxwell's equations in isotropic media. *IEEE Transactions on Antennas and Propagation,* 1966, vol. 14, p. 303–307.

[5] TAFLOVE, A., HAGNESS, S. C. *Computational Electromagnetics: The Finite-Difference Time-Domain Method*. 2nd ed. Boston, MA: Artech House, 2000, p. 552–558.

[6] HARMS, P. H., RODEN, A., MALONEY, J., KESLER, M., KUSTER, E., GEDNEY, S. D. Numerical analysis of periodic structures using the split field update algorithm. In *The Thirteenth Annual Review of Progress in Applied Computational Electromagnetics*. Monterey (CA), 1997.

[7] COLLIN, R. *Field Theory of Guided Waves*. Willey and IEEE Press p. 90–91.

About Authors

Nader FARAHAT is Associate Professor in the Electrical Engineering Department of the Polytechnic University of Puerto Rico. He is also adjunct research associate at the Pennsylvania State University.

Raj MITTRA is Professor in the Electrical Engineering Department of the Pennsylvania State University and the Director of the Electromagnetic Communication Laboratory. He is also the President of RM Associates, which is a consulting organization that provides services to industrial and governmental organizations, both in the U. S. and abroad.

Katherine LUGO is Master Student in the Electrical Engineering Department of Polytechnic University of Puerto Rico. She has received her Bachelor degree in Electronic Engineering from Universidad del Norte (Barranquilla, Colombia) in March 2006.

Lai-Ching MA received the B.S. and M.Phil. degrees in physics (minor in mathematics) from the Chinese University of Hong Kong, Hong Kong in 1996 and 2001, respectively, and the Ph.D. degree in electrical engineering from the Pennsylvania State University at University Park, PA, in 2008. Since 2002, she has held a graduate research assistantship at the Electromagnetic Communication Laboratory, Pennsylvania State University. Her research interests are in the area of antennas and computational electromagnetics with emphasis on the parallel finite difference time domain (FDTD) technique and its application to model and design the metamaterial/antenna or EBG/antenna composites for enhancing the antenna performance. She has received the 2008 A. J. Ferraro Graduate Research Award in recognition of excellence in Ph.D. research in the area of Electromagnetic Remote Sensing, Communications and Space Sciences at Pennsylvania State University.

Rodney A. GOMEZ is Master Student in the Electrical Engineering Department of Polytechnic University of Puerto Rico. He received his Bachelor degree in Electronic Engineering from Universidad del Norte (Barranquilla, Colombia) in March 2006.